JOURNAL OF CATALYSIS 74, 361–372 (1982)

Sulfonated Poly(styrene-divinylbenzene) Catalysts

II. Diffusion and the Influence of Macroporous Polymer Physical Properties on the Rate of Reesterification

K. M. DOOLEY, J. A. WILLIAMS, B. C. GATES,[1] AND R. L. ALBRIGHT*

*Center for Catalytic Science and Technology, Department of Chemical Engineering, University of Delaware, Newark, Delaware 19711, and *Rohm and Haas Company, Philadelphia, Pennsylvania 19105*

Received July 16, 1981; revised December 7, 1981

Macroporous polymer catalysts consist of aggregates of gelular microparticles interspersed with macropores. A set of macroporous, sulfonated, crosslinked polystyrene catalysts has been prepared, the crosslinking, surface area, and average macropore diameter having been varied independently. The catalysts were tested in a reaction involving molecules of intermediate size and polarity, the reesterification of ethyl acetate with *n*-propanol. Reaction rate data, measured at 106°C and 1 atm, demonstrate that sites on the surfaces of the gel microparticles are less active than sites within the microparticles. The more highly crosslinked polymers offer greater resistance to diffusion in the microparticles but have the more active catalytic sites within the microparticles. The data are represented by a model accounting for diffusion in macropores, Langmuir adsorption on microparticle surfaces, diffusion/swelling in microparticles, and second-order reversible reaction within microparticles. The model accounts for variations in diffusion coefficients and microparticle volume caused by swelling of the microparticles. The reaction rates were strongly influenced by diffusion in the microparticles, but the effects of macropore diffusion and adsorption on microparticle surfaces were negligible.

INTRODUCTION

Acidic ion-exchange resins consisting of sulfonated, crosslinked polystyrene are the only polymeric solids that have found large-scale applications as catalysts. The resins are used in a variety of processes, including olefin hydration (*1*), esterification (*2*), bisphenol A synthesis (*3*), and the methanol–isobutylene conversion to give methyl-*t*-butyl ether, a high-octane gasoline component (*4, 5*). Typical catalysts are macroporous, having BET surface areas as high as hundreds of square meters per gram and consisting of aggregates of polymer gel microparticles (microspheres) interspersed with macropores (*6*).

The first ion-exchange resins were swellable gel-form particles without true pores; these are usually less useful catalysts than macroporous resins, often being less stable. They are also often less active, since they require swelling by reactants or solvents; nonpolar reactants like hydrocarbons may not find access to catalytically active $-SO_3H$ groups in the interior of the gel, and polar solvents like water, which would swell the resin, may be inappropriate because they are strong inhibitors of the catalytic reactions. In macroporous catalysts, however, a large fraction of the $-SO_3H$ groups may be located close to the microparticle surfaces, therefore being accessible to nonpolar, nonswelling reactants.

Gel-form resins have been characterized by kinetics of simple reactions such as esterifications and alcohol dehydrations, and complications of intraparticle diffusion have sometimes been shown to be negligible by the lack of a particle size effect (*5, 7–9*). With macroporous resins, however, the more significant diffusion resistance is associated with the microparticles, the dimensions of which are almost un-

[1] To whom correspondence should be addressed.

0021-9517/82/040361-12$02.00/0

changed as particles are crushed. Consequently, there has been no systematic variation of microparticle dimensions—and therefore no quantitative characterization of the diffusion influence on catalysis by macroporous resins. It is clear, therefore, that there have been no demonstrated determinations of intrinsic kinetics with macroporous resin catalysts.

Several workers have attempted to elucidate the effects of resin crosslinking, but it has been difficult to vary crosslinking without producing a nonuniformly sulfonated resin (*10*). The concentration of acid groups in the resin may often be considerably less than the upper bound represented by monosulfonation of all the aromatic rings, and sometimes the rate of a catalytic reaction has been observed to increase with increasing resin crosslinking, since the diffusion-limited sulfonation process may result in the attachment of a larger fraction of $-SO_3H$ groups near the microparticle surfaces.

In this report, we summarize results obtained with a series of macroporous resin catalysts having systematically varied microparticle physical properties. The preparation of these catalysts is described elsewhere (*11*). Kinetics data were obtained for a reaction involving molecules of intermediate size and polarity, the reesterification of ethyl acetate with *n*-propanol:

$$CH_3\overset{\overset{O}{\|}}{C}-OCH_2CH_3 + CH_3CH_2CH_2OH \rightarrow CH_3\overset{\overset{O}{\|}}{C}-OCH_2CH_2CH_3 + CH_3CH_2OH \quad (1)$$

This reaction was chosen because the reactants and products are similar in size and tendency to swell the resin (*12*) and because kinetics can be measured simply. This reesterification reaction, among others catalyzed by sulfonated macroporous ion-exchange resins, has been investigated by Setínek and Beránek (*13*) and Zanderighi *et al.* (*14*). They fitted their kinetics data to second-order Langmuir–Hinshelwood rate equations, those commonly applied for esterifications, reesterifications, and ether syntheses from alcohols catalyzed by acidic surfaces (*15, 16*).

The resins used in this work were also used in a complementary study (*16*) of the catalytic dehydration of methanol to give dimethyl ether. Methanol was found to swell the resin strongly, and there was virtually no diffusion influence on the rate. Polymer physical properties were still found to be important—gel-form polymers being intrinsically more active catalysts than the macroporous resins. On the basis of molecular size and polarity, we expect the reactants in reesterification to exhibit less tendency than methanol to swell the resin; therefore, the plan was to collect data for this reaction in an attempt to establish structure–catalytic activity relations for macroporous resins with the resistance to diffusion in the microparticles being significant.

NOMENCLATURE

C	Concentration, mol/cm^3
d	Diameter, cm
D	Diffusivity, cm^2/s
k	Intrinsic reaction rate constant, cm^3/(mol · s)
K_{eq}	Reaction equilibrium constant
K_i	Adsorption equilibrium constant, atm^{-1}
l	Micropore length, cm
P	Pressure, atm
r	Reaction rate, mol/(cm^3 · s)
R	Rate of adsorption on microparticles, mol/(cm^3 · s)
$\bar{v}$	Partial molar volume, cm^3/mol
x	Fraction of surface acid groups
ϵ	Microparticle solute fraction
Φ	Generalized modulus
η	Effectiveness factor
ρ	Density, g/cm^3
θ	Concentration of acid groups, equivalents/g

Subscripts

ea	Ethyl acetate
p	Propanol
e	Ethanol
pa	Propyl acetate
$\mathcal{M}$	Macropore
M	Macroparticle
obs	Observed
μ	Microparticle

Superscripts

0	At center of or in unswollen state
s	Surface
	Effective

EXPERIMENTAL

The catalysts were macroporous, sulfonated poly(styrene-ethylvinylbenzene-divinylbenzene) resins specially made by the Rohm and Haas Company. Concentrations of exchangeable hydrogen ion in the resins were measured by titration; skeletal densities by helium–air pycnometry; apparent densities by mercury displacement under vacuum at 25°C; and BET surface areas by nitrogen adsorption–desorption at 77.3°K.

Reagent grade *n*-propanol and ethyl acetate were supplied by Fisher. The *n*-propanol was distilled from anhydrous K_2CO_3, and the ethyl acetate was dried over K_2CO_3 and then distilled from P_2O_5. Industrial grade helium (<15 ppm H_2O, 99.995% pure) was supplied by Linde.

Initial reaction rate data for the catalytic reesterification were determined with a packed-bed flow microreactor connected directly to the sampling valve of an Antek 300 gas chromatograph (GLC). Differential conversions were measured using ethyl acetate–*n*–propanol–helium feed mixtures as vapors at 106°C and 1 atm. Further details of the reactor system are described elsewhere (*16*).

A 2-mm-i.d., 1.83-m-long 316 stainless-steel GLC column of 80/100 mesh Chromasorb 101 was used to separate the product mixture. The column was temperature programmed with a 1-min initial hold at 110°C followed by a 15°C/min ramp to 185°C and a 5-min final hold. Helium carrier gas flow was 40 cm³/min. A flame ionization detector was used.

The GLC peaks were identified by coinjection of standards. Some reactor effluent samples were also separated and analyzed by GLC/ms; the mass spectra confirmed the identifications.

A fresh catalyst charge was added for each reaction experiment. Carbonaceous deposits were observed to have built up gradually on the used catalysts. The rate of the catalytic reaction decreased slowly with time on stream. The rates reported here are those extrapolated to zero onstream time.

RESULTS

The catalyst characterization data are summarized in Table 1. The concentrations of acid groups are nearly equal to values expected for uniform monosulfonation of all the phenyl rings, which indicates that the sulfonating reagent (H_2SO_4) penetrated the microparticles rapidly.

A reaction network accounting for the observed products and the expected catalytic reactions is shown in Fig. 1. The dominant reaction was the reesterification of *n*-propanol and ethyl acetate, giving *n*-propyl acetate and ethanol. Other reactions, listed in order of decreasing rate, are the dehydration of ethanol to give diethyl ether, the dehydration of *n*-propanol to give propylene, and the dehydration of ethanol to give ethylene. The rate of ethyl acetate hydrolysis was low and could not be measured because the acetic acid peak in the GLC trace was obscured by the neighboring peaks indicative of *n*-propanol and ethyl acetate. The oligomerization rates were not measured because the oligomers, also present in low concentrations, were eluted only slowly from the GLC column.

The most accurate measure of the reesterification rate is provided by the conversion data for the *n*-propyl acetate product, since it did not react further. The less

TABLE 1

Catalyst Properties

Catalyst	$-SO_3H$ group content (meq/g)	Skeletal density (g/cm³)	Apparent density (g/cm³)	Specific surface area (m²/g)	Monomer composition (wt%)			ϵ_M	d_μ (Å)	$d_{\mathcal{M}}{}^c$ (Å)
					Styrene	EVB[a]	DVB[b]			
A	5.46 ± 0.12	1.500 ± 0.005	0.482 ± 0.005	24 ± 3	85.9	6.1	8.0	0.679 ± 0.004	1670 ± 210	2350 ± 300
B	5.25 ± 0.06	1.426 ± 0.005	0.460 ± 0.005	23 ± 3	71.8	12.2	16.0	0.677 ± 0.004	1830 ± 240	2560 ± 340
C	5.47 ± 0.14	1.410 ± 0.005	0.495 ± 0.005	11 ± 3	85.9	6.1	8.0	0.649 ± 0.004	3870 ± 1050	4770 ± 1300
D	5.54 ± 0.18	1.473 ± 0.005	0.709 ± 0.005	12.5 ± 3	85.9	6.1	8.0	0.519 ± 0.004	3260 ± 780	2340 ± 560

[a] EVB, ethylvinylbenzene.
[b] DVB, divinylbenzene.
[c] In the calculation of pore diameters, the macropores were modeled as cylinders and the microparticles as spheres.

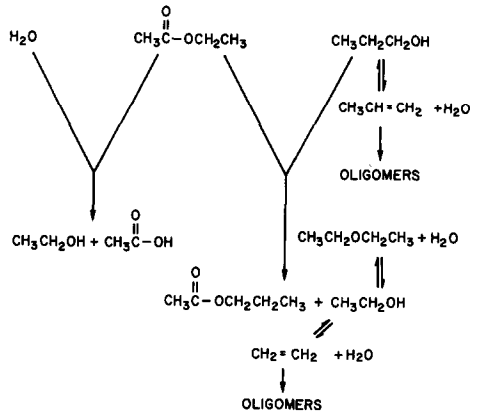

FIG. 1. Proposed reaction network for conversion of ethyl acetate and *n*-propanol catalyzed by sulfonic acid resins.

precise rate data determined from conversion to ethanol and its dehydration products are in good agreement with the rate data determined from *n*-propyl acetate analyses (Fig. 2).

The rates of reesterification reported below were determined from measured rates of *n*-propyl acetate formation as a function of time onstream in the flow reactor, as exemplified by the data Fig. 3. The curves demonstrate the occurrence of catalyst de-

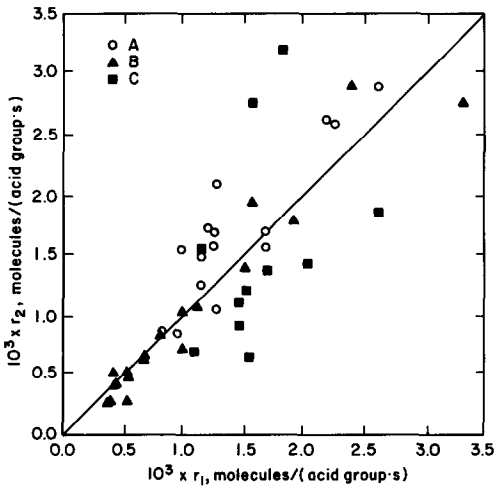

FIG. 2. Verification of mass balance. The rate r_2 is the rate of formation of ethanol plus twice that of diethyl ether plus that of ethylene, and r_1 is the rate of formation of *n*-propyl acetate. Data were obtained for catalysts A, B, and C (Table 1).

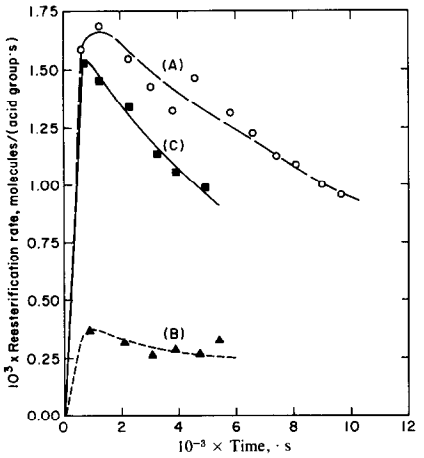

FIG. 3. Deactivation of the catalysts. Ethyl acetate partial pressure, 0.3 atm, *n*-propanol partial pressure, 0.1 atm.

activation. During the short initial period, the reactants were flowing from the feed pump to the catalyst and the catalyst particles were being swollen by the reactants. After the initial period, the rate was a maximum, and this value was considered to be representative of the fresh catalyst. Rates were measured in this way for a range of reactant partial pressures, and the data are summarized in Figs. 4–6.

If there were no influence of diffusion or swelling on the catalytic reaction rate, then the curves for the three catalysts would be expected to coincide. Since there are striking differences, we infer that swelling and transport phenomena need to be considered in modeling the catalyst performance.

DISCUSSION

Our goal is to explain the observed dependence of catalytic activity on polymer structure by accounting for swelling and transport effects. For reaction to occur between *n*-propanol and ethyl acetate, both

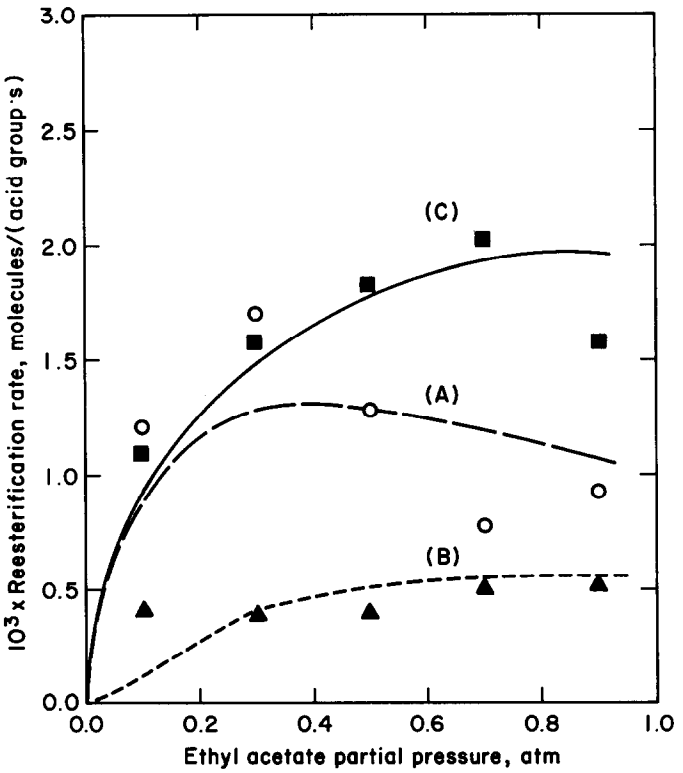

FIG. 4. Initial catalytic reaction rates. The *n*-propanol partial pressure was 0.1 atm. The curves are the fits to the data given by Eq. (13) with the optimum regression parameters of Table 4.

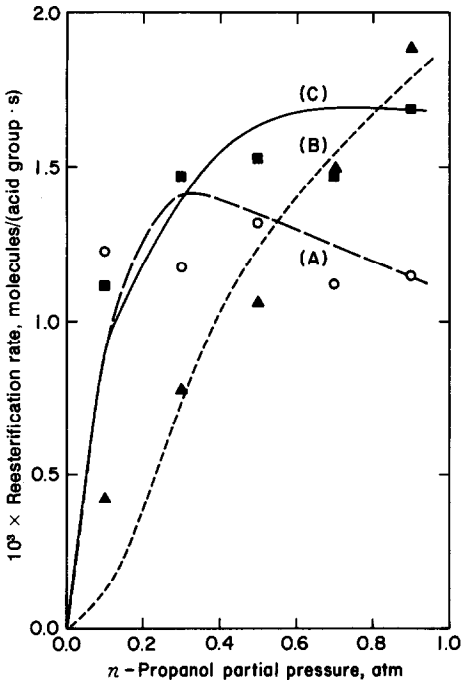

FIG. 5. Initial catalytic reaction rates. The ethyl acetate partial pressure was 0.1 atm. The curves are the fits to the data given by Eq. (13) with the optimum regression parameters of Table 4.

reactants must diffuse through the macropores, adsorb on the microparticles, and then swell the microparticles to find access to the catalytically active $-SO_3H$ groups. Changes in catalyst structure are expected to change the rates of the transport processes, and a model is proposed to account for the influence of these processes on the rate of the catalytic reaction.

Swelling and Reaction in the Polymers

The dependence of the observed rates on reactant partial pressures is shown in Figs. 4–6. These results lead to several qualitative inferences about the nature of the structure–catalytic activity relations:

(1) At low partial pressures of either reactant, rates of the catalytic reaction in the highly crosslinked catalyst (B) were lower than those observed for the other catalysts. This result suggests a substantial resistance to transport of reactants associated with the polymer network in B.

(2) At higher reactant partial pressures, however, catalyst B was as active as the others, which suggests that it was strongly swelled under these conditions.

(3) There appears to be a difference in the relative swelling rates of ethyl acetate and *n*-propanol that is crosslink dependent. The shapes of the rate-reactant partial pressure curves (Figs. 4 and 5) are about the same for catalysts A and C. These results suggest that, for either catalyst, the two reactants swell the polymer equivalently. However, ethyl acetate evidently swells catalyst B more strongly than does *n*-propanol, as indicated by the greater self-inhibition by ethyl acetate (Fig. 4) compared with *n*-propanol (Fig. 5).

(4) Higher microparticle surface area does not necessarily imply higher catalytic activity. Catalyst A, with high surface area and low crosslinking, is less active than C. Catalyst C contains the largest number of easily accessible catalytic sites in the microparticle interior, as evidenced by its high $-SO_3H$ group content, low surface area, and low crosslinking (Table 1).

The difference in the swelling characteristics of ethyl acetate and *n*-propanol in the 16% crosslinked catalyst B is an unexpected result. Wolf (*12*) found that alcohols and esters from the liquid phase were equivalent in their tendency to swell a catalyst similar to B. Setínek and Beránek (*13*) found that the equilibrium constants for adsorption of ethyl acetate and *n*-propanol at 120°C and 1 atm were similar. We explain the higher rate of swelling by ethyl acetate than by *n*-propanol as a consequence of the weaker polar interaction of the ester with the $-SO_3H$ groups. More polar molecules, such as the alcohol, are restricted more by the acid groups in the small, rigid micropores of highly crosslinked polymers.

Supporting evidence for the interpretation of the behavior of catalyst B at higher reactant partial pressures is provided by several references (*8, 10, 17–19*), which

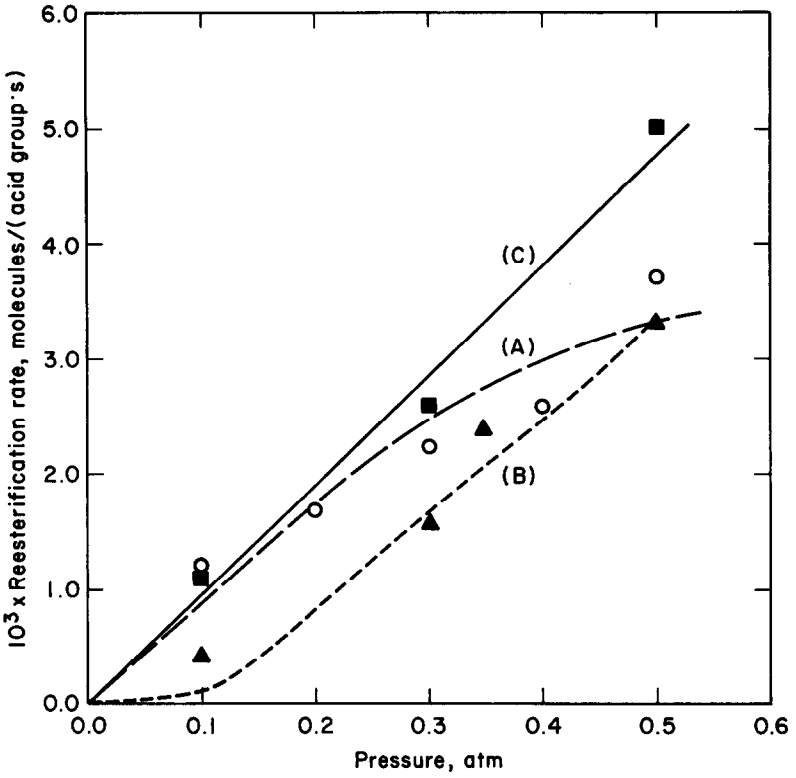

FIG. 6. Initial catalytic reaction rates determined with equal partial pressure of the reactants. The curves are the fits to the data given by Eq. (13) with the optimum regression parameters of Table 4.

demonstrate that, under these conditions, as resin crosslinking increases, so do the rates of several acid-catalyzed reactions—up to a point. Further increases to >20% crosslinking produce catalysts so rigid that swelling is virtually impossible, and rates decrease. Additional evidence is provided by literature (*20*) results for isopropanol dehydration catalyzed by crosslinked sulfonated polystyrene membranes. These results follow the same pattern as our data; a 5% crosslinked catalyst is much more active than an 8% crosslinked catalyst at low isopropanol partial pressures, whereas at higher partial pressures, the 8% crosslinked catalyst is slightly more active. This rate behavior may be ascribed in part to the previously mentioned nonuniformity of sulfonation, but we infer that this is not the only cause, since in many cases the resins were relatively uniform even at high crosslinking, and the membranes were certainly uniform.

As crosslinking increases, the more rigid polymer matrix is expected to increasingly restrict the orientation (hydrogen bonding) of $-SO_3H$ groups. At the same time there is an increased electrostatic repulsion of $-SO_3H$ groups because they are more closely spaced in the more highly crosslinked polymer. Consequently, the strength of interaction of the acid groups with reactant molecules is decreased (*21*, *22*). For strongly hydrogen-bonded molecules, such as *n*-propanol, the decrease is slight, whereas for the less polar ethyl acetate, it is considerable. But it is this decrease in the strength of bonding of reactant to $-SO_3H$ groups that may account for the maximum in catalytic activity as a function of crosslinking at high degrees of swelling.

The high activity of the low-surface-area

catalyst C is attributed to the higher activities of $-SO_3H$ groups in the interior of the microparticles. Several authors (e.g., *9, 18*) have observed orders of reaction in $-SO_3H$ groups that are greater than one, indicating the involvement of a hydrogen-bonded network of $-SO_3H$ groups forming the catalytic sites (*20*). These results lead to the inferences that (i) sites on the surface of a microparticle are less active than those in the interior and (ii) that an effectively swelled gel-form resin may be more active than a macroporous resin of equal crosslinking. The results given in an accompanying paper (*23*) (characterizing the dehydration of methanol catalyzed by both kinds of polymers) support this interpretation.

Model Development

Results of calculations by standard methods have shown that concentration and temperature gradients external to the catalyst particles and temperature gradients within the particles were negligible in the experiments reported here (*15, 24*). The concentration gradient associated with the macropores could not be estimated directly, since the complete rate equation was unknown. Instead, macropore diffusion resistance was gauged using Bischoff's generalized model accounting for diffusion with reaction in a permeable catalyst particle (*25*). According to the model, the dimensionless modulus Φ is

$$\Phi = \frac{r_{obs} L^2 r(C_M^s)}{2\int_{C_{eq}}^{C_M^s} D_M'(C)\, r(C)\, dc} \cdot \qquad (2)$$

For an irreversible first-order reaction, this reduces to the well-known Weisz modulus:

$$\Phi = \frac{r_{obs} d_M^2}{36 D_M' C_M^s} \cdot \qquad (3)$$

For a second-order reversible reaction, the generalized modulus reduces to

$$\Phi = \frac{3\, r_{obs} d_M^2 C_M^s}{72 D_M'(C_M^{s3} - C_{eq}^3)} \cdot \qquad (4)$$

The criterion for negligible macropore diffusion resistance is $\Phi \ll 1$. For second-order reversible Langmuir–Hinshelwood kinetics, the exact value of the modulus would lie between the values calculated from Eqs. (3) and (4). The results of the calculations for the extreme case of maximum observed rates and macropore lengths are summarized in Table 2. The equilibrium concentration C_{eq} was calculated from experimental results. All the moduli were calculated to be ≤ 0.009, which indicates that the concentration gradients were insignificant. Therefore, in the following analysis, the reactant concentration external to any microparticle is assumed to be equal to the bulk gas-phase concentration.

TABLE 2

Calculated Generalized Moduli[a]

Catalyst	$10^3 \times$ Modulus Eq. (3)	$10^3 \times$ Modulus Eq. (4)
A	3.9	6.4
B	3.1	5.0
C	5.3	8.3

[a] The moduli were calculated from the data of Table 1 and Figs. 4–6. Details are given elsewhere (*15*).

In the diffusion-reaction model of a resin particle, both macropore and micropore diffusion are accounted for, although in the absence of a significant macropore concentration gradient, only the micropore resistance could be tested by the data. The assumptions underlying the model include the following:

(1) The reactants and products are present in a vapor phase external to the catalyst particles.

(2) There is no reactant in the microparticles that is not chemisorbed (bonded to $-SO_3H$ groups), and chemisorption on microparticle surfaces precedes diffusion into the microparticles. In other words, it is assumed that no physically adsorbed reactants participate either in swelling or the catalytic reaction. The necessity of reactant chemisorption on a microparticle surface is confirmed by the poisoning data of Mar-

tinec *et al.* (*10*) and Setínek and Prokop (*26*), who found that only a small amount of base adsorption, shown to occur mainly on microparticle surfaces, rendered macroporous acid catalysts almost completely inactive. The same amount of poisoning was observed to deactivate a gel-form catalyst totally.

(3) Product adsorption on microparticle surfaces is negligible.

(4) The reaction of ester with alcohol, both being bonded to $-SO_3H$ groups, is rate determining. This assumption is in agreement with reported catalytic kinetics (*13, 14*). The chemisorption of reactants on microparticle surfaces is ruled out as a rate-determining step because of the observed lack of an influence of this surface area on rate.

(5) Langmuir adsorption occurs on the microparticle surfaces.

With these assumptions, the relevant equations follow from the swelling and hydration theory of Lal and Douglas (*27*), the resin diffusion results of several workers, especially Mackie and Meares (*28*) [other results are summarized by Meares (*29*)], and the theory of the generalized modulus.

The volumes of polymers swelled with water have typically been observed to increase linearly with small amounts of added water (*27*). Therefore,

$$\epsilon_\mu = \bar{v} C_\mu. \tag{5}$$

The solute (adsorbate) fraction is also dependent on the crosslinking, since the partial molar volume of the solute is a weak function of crosslinking. Equation (5) is probably even more applicable to our data than to water, since alcohols and esters swell and associate with acid groups to a lesser degree than does water.

The effective diffusivity of the solute in a highly swollen resin has been represented by the following equation (*28, 29*):

$$D'_\mu = \left(\frac{\bar{v} C_\mu}{2 - \bar{v} C_\mu}\right)^2 D. \tag{6}$$

This expression is based on a homogeneous polyelectrolyte gel model, according to which all diffusion paths are equivalent for both polymer and solute, and according to which the random diffusive transport is independent of polar interactions with the polymer chains. This is an inexact approximation for our vapor-phase reactants, relatively rigid polymer chains, and strong polar interactions in the smallest pores, but it is the only available expression based on a wide variety of data for acidic ion-exchange resins. It reduces to the correct limit ($D'_\mu \to D$) as the reciprocal partial molar volume approaches the solute concentration in the microparticles.

If it were possible to observe the catalytic reaction rate just outside a microparticle, it would be

$$r_{\mu \mathrm{obs}} = \eta_\mu r\,(C_\mu^{\,s}) = \frac{\left[2 \int_{C_\mu^{\,0}}^{C_\mu^{\,s}} D'_\mu(C) r(C) dC\right]^{1/2}}{l}. \tag{7}$$

For strong diffusion limitations, $C_\mu^{\,0} = C_{\mathrm{eq}}$. The diffusion path length l increases as swelling occurs. Since the crosslinks strongly restrict the polymer chains, it is assumed that the total unswollen microparticle surface area equals the swollen microparticle surface area. The path length then becomes

$$l = \frac{d_\mu}{6} = \frac{d_\mu^{\,0}}{6(1 - \epsilon_\mu^{\,s})^{1/2}}. \tag{8}$$

It remains to couple Eq. (7) for microparticles with the rate, adsorption, and macropore diffusion equations. Consistent with the literature reports of second-order kinetics (*13, 14*), the rate equation for reaction within the microparticles is taken to be

$$r = k\left(C_{\mu \mathrm{p}} C_{\mu \mathrm{ea}} - \frac{1}{K_{\mathrm{eq}}} C_{\mu \mathrm{e}} C_{\mu \mathrm{pa}}\right). \tag{9}$$

The concentration of reactant adsorbed on the microparticle surface is as follows, provided that *n*-propanol is the limiting reactant (if ethyl acetate is the limiting reactant, the equation is analogous):

$$C_{\mu p}^{s} = \theta x \rho_{\mu}^{0}(1 - \epsilon_{\mu}^{s}) \times \left(\frac{C_p}{1/K_p + C_p + (K_{ea}/K_p)C_{ea}}\right). \quad (10)$$

The fraction of surface sites, x, for each catalyst, was calculated as in Ref. (*15*). To couple microparticle diffusion-reaction to macropore diffusion, we note that in the macropores the rate of adsorption on the microparticles equals the reaction rate inside the microparticles. Therefore,

$$r_{obs} = \eta_M R(C_M^s) = \left[2\int_{C_M^0}^{C_M^s} D'_M(C)R(C)dC\right]^{1/2} \Big/ (d_M/6). \quad (11)$$

$$R(C) = r_{\mu obs}(1 - \epsilon_M). \quad (12)$$

Combining Eqs. (5)–(12) and assuming $r_{\mu obs} \simeq r_{obs}$ (consistent with the calculated macropore concentration gradients) gives

$$r_{obs} = \frac{\left[2\int_{C_{eq}}^{C_{\mu p}^{s}} kD_p\left(C_{\mu p}C_{\mu ea} - \frac{1}{K_{eq}}C_{\mu e}C_{\mu pa}\right)\left(\frac{\epsilon_\mu}{2 - \epsilon_\mu}\right)^2 dC_{\mu p}\right]^{1/2}}{\left(\frac{d_\mu^0}{6}\right)(1 - \epsilon_\mu^s)^{1/2}}. \quad (13)$$

where

$$\epsilon_\mu^s \simeq \bar{v}_p C_{\mu p}^s + \bar{v}_{ea} C_{\mu ea}^s. \quad (14)$$

$$\epsilon_\mu = \bar{v}_p C_{\mu p} + \bar{v}_{ea} C_{\mu ea} + \bar{v}_{pa} C_{\mu pa} + \bar{v}_e C_{\mu e}. \quad (15)$$

These equations were used in a regression analysis with all the reesterification kinetics data. There are seven unknown parameters, k, K_p, K_{ea}/K_p, and the four partial molar volumes. Estimates of the ranges of all of these except k (Table 3) allowed us to reduce the problem to essentially a linear regression for k, except for the variation of the rest of the unknowns within their constraints.

TABLE 3

Assumed Ranges of Parameters in Eq. (13)

Parameter	Value
K_p	0.0–25.0 atm^{-1}
K_{ea}/K_p	0.0–10.0
$\bar{v}$	100–12,000 cm^3/mol[a]
	100–4,700 cm^3/mol[b]
	100–27,000 cm^3/mol[c]

[a] Catalyst A.
[b] Catalyst B.
[c] Catalyst C.

The maximum adsorption equilibrium constants (Table 3) correspond to the maximum literature values for acidic resins (*7, 10, 13, 14, 30*). The minimum partial molar volumes are approximately the saturated liquid volumes; the maximum volumes were estimated from Lal and Douglas' (*27*) determinations of the maximum porosities in hydrated resins which were used with Eqs. (10) and (14), as the adsorption equilibrium constants approached infinity. For finite values of these constants, the maximum partial molar volumes are a few percent greater. In the regression analysis, all component partial molar volumes were assumed equal; $\bar{v}$ represents an average value.

After a grid search, the $k - K_p - K_{ea}/K_p$ response surface for each catalyst at three different values of $\bar{v}$ was plotted. The standard error of k was used to choose the best estimates of K_p, K_{ea}/K_p, and $\bar{v}$. The optimum regression coefficients and their confidence limits are given in Table 4 for each catalyst. The computations showed that this was a true global optimum, implying convergence to these optimum values whatever constraints were set on the parameters. The confidence limits are based on the approximate 95% critical contours of

TABLE 4

Results of Regression Analysis

Catalyst	$\bar{v}$ (cm³/mol)	K_p (atm⁻¹)	K_{ea}/K_p	$k^{1/2}$ [a] (cm³/mol · s)$^{1/2}$
A	100	3.5 ± 2.0	0.75 ± 0.27	(0.90 ± 0.24) × 10^3
B	100	0.50 ± 0.25	2.0 ± 0.7	(5.4 ± 2.7) × 10^3
C	100	1.4 ± 0.9	0.50 ± 0.25	(4.6 ± 2.9) × 10^4

[a] As seen from Eq. (13), $k^{1/2}$ is obtained from the regression. The corresponding best values of k are 8.1 × 10^5, 2.9 × 10^7, and 2.1 × 10^9 cm³/(mol · s) for A, B, and C, respectively.

the response surfaces. The limits in some cases are large, reflecting the scatter of the kinetics data, the uncertainties of the model, the difficulty in regression with the number of parameters involved, and the difficulties in analyzing diffusion and adsorption phenomena from reaction data alone. Although the statistical differences between optimum values at different average partial molar volumes are not significant, there is a definite trend toward less error for volumes in the saturated liquid region (≈100 cm³/mol). Also, for two of the catalysts, A and B, the model breaks down at $\bar{v} > 1000$ cm³/mol, since the regression intercept deviates from its expected value of zero. Therefore, the lower partial molar volumes seem more appropriate.

The quantitative results reenforce the qualtitative conclusions about the nature of the effects of polymer properties on catalytic activity. The catalysts having low surface area (C) and high crosslinking (B) both show a high intrinsic rate constant compared with that of the low crosslinking, high surface area catalyst A. The latter has the largest adsorption equilibrium constants, as expected. The magnitudes of the adsorption equilibrium constants agree well with literature values (*13, 14, 30*) of about 0.6–2.0 atm^{-1} at nearly equal temperatures.

The catalytic rate data cannot be described adequately by models that ignore microparticle swelling. For example, a number of second-order Langmuir–Hinshelwood rate equations were used to regress the rate data (*15*). Aside from squared errors at least 50% larger than those predicted by the present model, the simple Langmuir–Hinshelwood models predicted zero or negative adsorption equilibrium constants for catalyst B.

In summary, we conclude that this model provides a proper framework for interpretation of catalytic reaction rate data for macroporous polymers.

REFERENCES

1. Akiyama, S., *Chem. Eng.* 56 (1973).
2. Davini, P., and Tartarelli, R., *Chim. Ind. (Milan)* **53,** 1119 (1973).
3. Kwantes, A., and Gautier, P. A., U.S. Pat. 4,191,843 (1980).
4. Ancillotti, F., Massi Mauri, M., Pescarollo, E., and Romagnoni, L., *J. Mol. Catal.* **4,** 37 (1978).
5. Rozhkov, S. V., Bobylev, B. N., Farberov, M. I., and Rabotnova, M. I., *Kinet. Katal.* **18,** 1429 (1977).
6. Pitochelli, A. R., "Ion Exchange Catalysis and Matrix Effects." Rohm and Haas Company, Philadelphia, 1975.
7. Bhatia, S., Rajamani, K., Najkhowa, P., and Gopala Rao, M., *Ion Exchange Membranes* **1,** 127 (1973).
8. Frilette, V. J., Mower, E. B., and Rubin, M. K., *J. Catal.* **3,** 25 (1964).
9. Gates, B. C., and Johanson, L. N., *J. Catal.* **14,** 69 (1969).
10. Martinec, A., Setínek, K., and Beránek, L., *J. Catal.* **51,** 86 (1978).
11. Albright, R. L., Dooley, K. M., and Gates, B. C., to be published.
12. Wolf, F., *in* "Ion Exchange in the Process Industries," p. 285. Society of Chemical Industry, London, 1969.
13. Setínek, K., and Beránek, L., *J. Catal.* **17,** 306 (1970).

14. Zanderighi, L., Setínek, K., and Beránek, L., *Coll. Czech. Chem. Commun.* **35,** 2367 (1970).
15. Dooley, K. M., Ph.D. thesis, Univ. of Delaware, Newark, DE, in preparation.
16. Diemer, R. B., Jr., M.Ch.E. thesis, Univ. of Delaware, Newark, DE, 1980.
17. Andrianova, T. I., *Kinet. Katal.* **5,** 927 (1964).
18. Gates, B. C., Wisnouskas, J. S., and Heath, H. W., Jr., *J. Catal.* **24,** 320 (1974).
19. Heath, H. W., Jr., and Gates, B. C., *Amer. Inst. Chem. Eng. J.* **18,** 321 (1972).
20. Thornton, R., and Gates, B. C., *J. Catal.* **34,** 275 (1974).
21. Saldadze, K. M., Kopylova, V. D., Kargman, V. W., and Galitskaya, N. B., *J. Polym. Sci.* Symp. **47,** 309 (1974).
22. Kopylova, V. D., Kargman, V. B., Suvorova, L. N., Galitskaya, N. B., and Saldadze, K. M., *Vysokomol-Soyed.* **A15,** 460 (1973).
23. Diemer, R. B., Jr., Dooley, K. M., Gates, B. C., and Albright, R. L., *J. Catal.* **74,** 373 (1982).
24. Froment, G. F., and Bischoff, K. B., "Chemical Reactor Analysis and Design." Wiley, New York, 1979.
25. Bischoff, K. B., *Amer. Inst. Chem. Eng. J.* **11,** 351 (1965).
26. Setínek, K., and Prokop, Z., *Coll. Czech. Chem. Commun.* **41,** 1282 (1976).
27. Lal, B. B., and Douglas, W. J. M., *Ind. Eng. Chem. Fund.* **13,** 223 (1974).
28. Mackie, J. S., and Meares, P., *Proc. R. Soc.* **A232,** 498 (1955).
29. Meares, P., *in* "Diffusion in Polymers" (J. Crank and G. S. Park, Eds.). Academic Press, London, 1968.
30. Yeramian, A. A., Gottifredi, J. C., and Cunningham, R. E., *J. Catal.* **12,** 257 (1968).